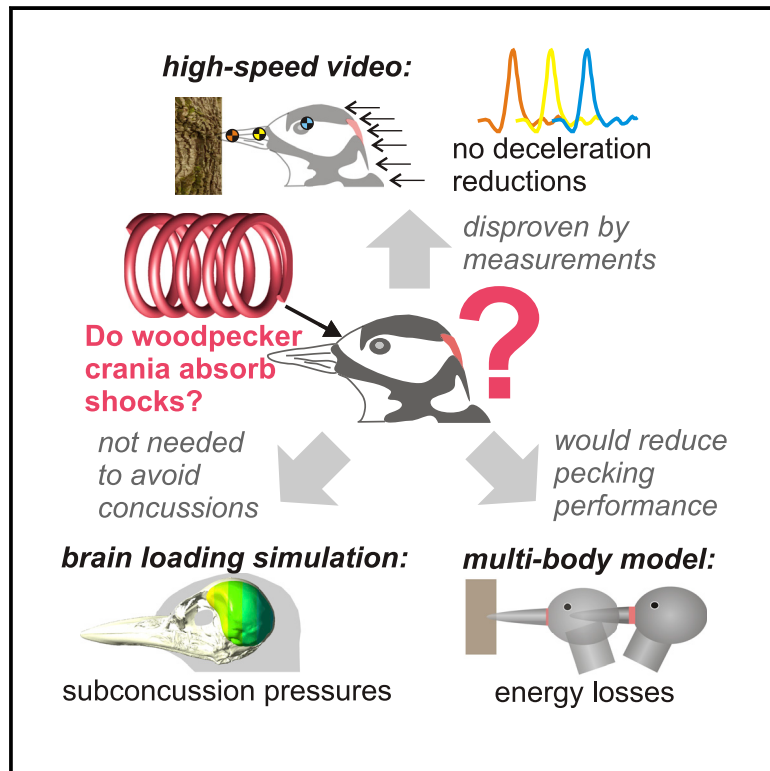# Current Biology

Woodpeckers minimize cranial absorption of shocks

Graphical abstract

Authors

Sam Van Wassenbergh,
Erica J. Ortlieb, Maja Mielke,
Christine Böhmer, Robert E. Shadwick,
Anick Abourachid

Correspondence

sam.vanwassenbergh@uantwerpen.be

In brief

Van Wassenbergh et al. use high-speed
video analyses and biomechanical
models to show that woodpecker heads
do not function as shock absorbers as
commonly assumed, but as stiff hammers
to aid pecking performance.

Highlights

- Woodpecker heads behave very stiffly during *in vivo* pecking impacts

- Shock deceleration of the braincase is not reduced relative to the beak

- Absence of cranial shock absorption is adaptive to improve pecking performance

- Inertial loading of woodpecker brains is below primate concussion thresholds

 CellPress

Report

Woodpeckers minimize cranial absorption of shocks

Sam Van Wassenbergh,[1,2,6,7,*] Erica J. Ortlieb,[3] Maja Mielke,[1] Christine Böhmer,[2,4,5] Robert E. Shadwick,[3] and Anick Abourachid[2]

[1]Laboratory of Functional Morphology, Department of Biology, University of Antwerp, Universiteitsplein 1, 2610 Antwerpen, Belgium
[2]UMR 7179 C.N.R.S/M.N.H.N., Département Adaptations du Vivant, 57 rue Cuvier, Case Postale 55, 75231 Paris Cedex 05, France
[3]Department of Zoology, University of British Columbia, 6270 University Boulevard, Vancouver, BC V6T 1Z4, Canada
[4]Department für Geo- und Umweltwissenschaften und GeoBio-Center, Ludwig-Maximilians-Universität München, Richard-Wagner-Straße 10, 80333 München, Germany
[5]Zoologisches Institut, Christian-Albrechts-Universität zu Kiel, Am Botanischen Garten 1-9, 24118 Kiel, Germany
[6]Twitter: @UAFunMorph
[7]Lead contact
*Correspondence: sam.vanwassenbergh@uantwerpen.be
https://doi.org/10.1016/j.cub.2022.05.052

SUMMARY

The skull of a woodpecker is hypothesized to serve as a shock absorber that minimizes the harmful deceleration of its brain upon impact into trees[1–11] and has inspired the engineering of shock-absorbing materials[12–15] and tools, such as helmets.[16] However, this hypothesis remains paradoxical since any absorption or dissipation of the head's kinetic energy by the skull would likely impair the bird's hammering performance[4] and is therefore unlikely to have evolved by natural selection. *In vivo* quantification of impact decelerations during pecking in three woodpecker species and biomechanical models now show that their cranial skeleton is used as a stiff hammer to enhance pecking performance, and not as a shock-absorbing system to protect the brain. Numerical simulations of the effect of braincase size and shape on intracranial pressure indicate that the woodpeckers' brains are still safe below the threshold of concussions known for primate brains. These results contradict the currently prevailing conception of the adaptive evolution of cranial function in one of nature's most spectacular behaviors.

RESULTS

The forceful impact of the beak and the associated abrupt deceleration of woodpeckers' heads when hammering into trees for feeding and nesting, or when drumming for interspecific communication[17] has long intrigued scientists who wonder how these birds protect their brain against injury.[1,4–11,18–21,4,18–21] When a moving head strikes a stationary object, the sudden deceleration of the head will cause compressions (or positive pressures) at the impact site of the brain (coup region) and expansions (or negative pressure) at the back side (contrecoup region), which can both damage neurons and cause dysfunction.[22] A straightforward way to decrease these harmful decelerations (i.e., shocks) of the brain is to absorb or dissipate the head's kinetic energy during impact in a compliant material (i.e., a shock absorber) located between the brain and the impact site, as, for example, in airbags or bike helmets. This diminishing of shock impulses is fundamentally different from other types of protective adaptations such as rigid body amours that withstand high local forces.

Since the lifestyle of woodpeckers inevitably subjects these birds to high decelerations of the head,[20] multiple studies have sought adaptations related to shock absorption within the cranial musculoskeletal system of woodpeckers.[1–3,12,23] The spongy bone in a woodpecker's skull, which is particularly well developed at the frontal region of the skull just posterior to the naso-frontal joint between the upper beak and the braincase (Figure 1), has been identified as a prime candidate for shock absorption.[10,12,13] Impact energy could also be absorbed through eccentric or isometric contraction of the protractor muscles of the quadrate and lower beak (e.g., *musculus protractor pterygoidei*) if the lower beak is pushed posteriorly relative to the skull when impacting a tree.[1,2,3] Despite the lack of evidence for biologically significant shock absorption during pecking in woodpeckers, engineers of shock-absorbing materials[12–15] and tools, such as helmets,[16] have used the morphology of woodpeckers as a source of inspiration.

However, not only do these hypotheses on shock absorption by the cranial musculoskeletal system remain untested in a natural situation, but they are also controversial.[4,18,20] The reason for this controversy is the apparent paradox of absorbing the shock the woodpecker wants to impart on the tree. In other words, as written by May and colleagues,[4] if the beak absorbed much of its own impact the unfortunate bird would have to pound even harder. Consequently, as a strong selective pressure has probably improved hammering performance through the evolution of woodpeckers, how can a trait that reduces this performance have evolved as well?

In vivo impact kinematics

Our first aim was to test the long-standing hypothesis stating that shock absorption is occurring between beak and brain so that the deceleration of the brain is significantly reduced compared with the deceleration of the beak upon impact. We managed to capture high-speed videos of six individuals from three species
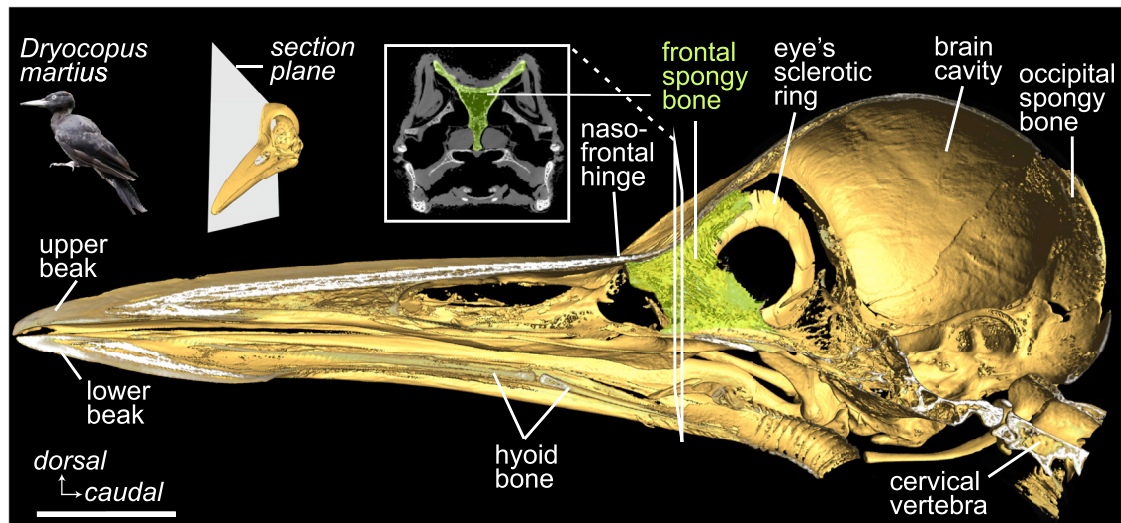
Figure 1. Cranial bone of *Dryocopus martius*

Figure360▷ For a Figure360 author presentation of figure 1, see the figure legend at https://doi.org/10.1016/j.cub.2022.05.052.

The well-developed zone of spongy bone at the frontal region of the skull, which is hypothesized to absorb shocks, is highlighted in green in this medial view on the right side of the skull (3D reconstruction from a CT scan). A cross-section through the frontal bones is shown in the upper center of the figure. Scale bars, 20 mm.

(2× *Dryocopus martius*, 2× *Dryocopus pileatus*, 2× *Dendrocopos major*) kept in aviaries as they hammered into wood. We used 109 videos to perform frame-by-frame tracking of two landmarks on the beak, one on the eye (Figure S1) and, additionally for *D. pileatus*, a painted dot on the skin covering the skull posterior of the eye. Since the eyes are tightly packed in the skull's orbits, which fill the space in between the frontal spongy bone and the anterior side of the braincase (Figure 1), eye deceleration will closely approximate the deceleration of the anterior side of the braincase. This is confirmed by the nearly identical mean decelerations of the eye versus skull markers in *D. pileatus* (+1.1%; two-tailed paired t test: $t_{df23} = -0.28$; p = 0.79).

The results of the kinematic analysis of *in vivo* pecking (Figures 2 and S2) show that the zone connecting the beak and eye landmarks behaved stiffly in all individuals studied (Video S1). The mean peak decelerations either did not differ significantly between eye and beak, as in *D. martius* and in one individual of *D. major*, or were significantly higher at the eye than at the beak as in *D. pileatus* and in the other individual of *D. major* (Figure 2A; Table S1). Next, the relationship between deceleration of the landmark tracking the middle of the beak (x axis) and the landmark of the eye (y axis) was analyzed further (Figure 2B). Hypothetical linear regression slopes of x against y of 1 would be analogous to the behavior of a rigid interface between beak and braincase, while 0 would imply a complete absorption of the shock in between these two landmarks. Reduced major axes regression slopes of the six individuals studied ranged from 0.966 to 1.308 (Figure 2B). This indicates that shock absorption was either negligibly small (3.3% deceleration reduction in *D. martius* individual 2) or absent (slopes > 1 in all other individuals). The small amount of compression observed between the beak and braincase markers around the time of impact in *D. pileatus* and *D. major* (Figures S2D–S2F) clearly did not result in a notable deceleration reduction for the braincase.

No adaptive value of shock absorption by the cranium

In order to understand why little or no shock absorption was observed from an adaptive perspective, our second objective was to quantify the functional implications of varying the degree of cranial shock absorption on the bird's hammering performance and reducing brain deceleration. This was done by biomechanical modeling of *D. martius* based on anatomical measurements, as well as two variables obtained from our kinematic analysis: the average speed of the head at impact (used as a target value to fine-tune the impulse applied to the head) and the beak's deceleration duration (used as a target value to fine-tune the mechanical characteristics of the wood). A linear spring connected the modeled beak to the braincase, and its compression allowed the deceleration of the braincase to be attenuated (Figure 3A). As a measure for hammering performance, penetration into wood was calculated following the theoretical physics of driving a nail into wood[24] (Figure S3).

These model simulations confirmed that absorbing part of the kinetic energy of the head into a compressing elastic structure during impact would significantly reduce the penetration of the beak into the tree (Figure 3B). This result could be predicted a priori from the principle of energy conservation, but how does this affect brain deceleration? For relatively stiff beak-braincase interfaces that yield compressions below 1.5 mm, the benefit of such a compressing elastic structure for reducing peak deceleration of the brain was variable (green curves in Figure 3B) due to a complex mechanical interaction between the compressing elastic structure, the moving masses on both sides of it, and the force from the tree. For more compliant springs, brain deceleration would be reduced considerably, though at the expense of penetration depth (Figure 3B; Video S2).

For pecking with equal beak penetration depths, stiffer woodpecker crania required less work, as predicted previously based on the principle of energy conservation:[4] to peck equally deep, more kinetic energy input is required when part of this energy
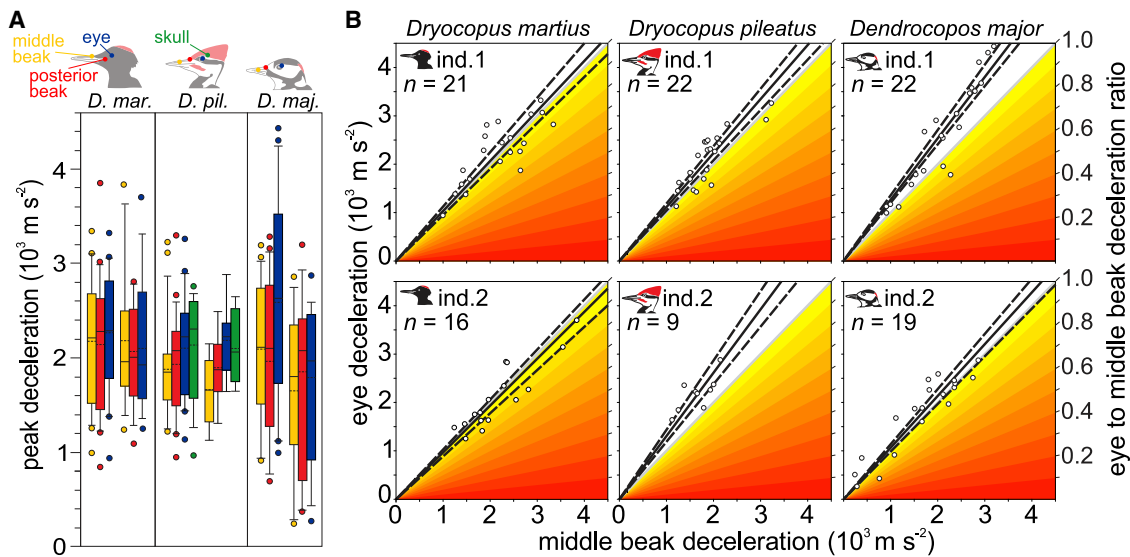
Figure 2. *In vivo* decelerations of the beak and braincase

Figure360▷ For a Figure360 author presentation of figure 2, see the figure legend at https://doi.org/10.1016/j.cub.2022.05.052.

(A) Boxplots of deceleration magnitude show the variance between hits for the four color-coded landmarks (middle beak, yellow; posterior beak, red; eye, blue; skull, green) in the three species studied (individual 1: left; individual 2: right; box boundaries: 25th and 75th percentiles; whiskers: 10th and 90th quartiles; spheres: data points outside 10th to 90th quartiles; line within box: median; dashed line: mean) (see Table S1 for statistical results and Figure S2 for time profiles).

(B) Relationship between middle beak and eye deceleration for each individual, showing linear regression lines (solid black lines), 95% confidence limits (dashed lines), and the equality line (gray; slope = 1). Iso-attenuations of deceleration (i.e., varying degrees of shock absorption) are color scaled from yellow (no shock absorption) to red (full shock absorption) as indicated on the right-side vertical axis (see Table S2 for statistical results).

See also Video S1.

becomes stored in compressing elastic tissues (Figure 3C; Video S2). Similar hits would thus require a higher energy expenditure from animals with cranial shock absorbers compared with those without. Interestingly, when shock-absorbing heads were impacting trees at increased velocities to equalize pecking performance, there was no benefit in terms of brain protection provided by a reduction in the braincase's deceleration (Figure 3C; green below zero). Under the current linear elastic behavior of our models, the compressing elastic structure delays the head's deceleration but causes a second deceleration peak around the time the head comes to a stop (Figure 3D). Our model predicts that, at this phase, the remaining kinetic energy of the head is dissipated at a high rate because the shock absorber is already loaded in compression and the resistance to further penetration of the beak into the tree is relatively high when the beak has already penetrated deep into the wood. Also, if the cranial compression would involve viscous damping instead of an elastic behavior, the braincase's deceleration does not decrease (Figure S4).

Brain inertial loading and safety factor

Finally, our morphological and kinematic data allow us to assess the severity of the observed head decelerations. Following previous theoretical work,[18,20,25] we used a comparative approach to evaluate the effect of shape and size of the braincase on intracranial pressure. Our computational model, assuming the braincase to be a water-filled, closed vessel under a purely inertial loading (i.e., without shape changes to the bony encasement), is conceptually simple but will nevertheless capture the basic mechanics of transient coup and contrecoup pressure gradients.[26] Intracranial

pressure for a typical, adult human braincase at the concussion threshold for sagittal-plane deceleration ($1,350$ m s^{-2})[27] was 103 kPa (coup) and -101 kPa (contrecoup) (Figure 4A). Even at the highest deceleration observed, woodpeckers *D. martius*, *D. pileatus*, and *D. major* would, respectively, experience only 60%, 39%, and 50% of this pressure (Figures 4B and 4C). This implies that, if overall protection mechanisms of the brain are similar to those of primates, the woodpeckers are operating around a "brain trauma safety factor" of about 2 (Figure 4C). This means these species would need to hit their selected spots twice as fast as observed or strike at its top speed on wood that is four times as stiff to suffer a concussion.

DISCUSSION

Together, these results reveal that the heads of woodpeckers function as stiff hammers during pecking. This is explained by the demonstrated lack of adaptive value of evolving a built-in shock absorber (Figures 3C and S4C). Consequently, the zones of spongy bone at both the coup and contrecoup side of the braincase (Figure 1) probably serves an important role in "resisting" impact forces without failing[23,28] rather than "absorbing" impact energy by elastic deforming.

Our simulations of intracranial pressures confirm Gibson's[18] theory that such a system could function without "special" protections against mechanical brain trauma for the behavior quantified in our study species. From an evolutionary point of view, however, limits will probably apply to head size, maximal strike speed, and hardness of selected trees,[29] or any combinations thereof, as increasing these factors will make brain trauma more likely by
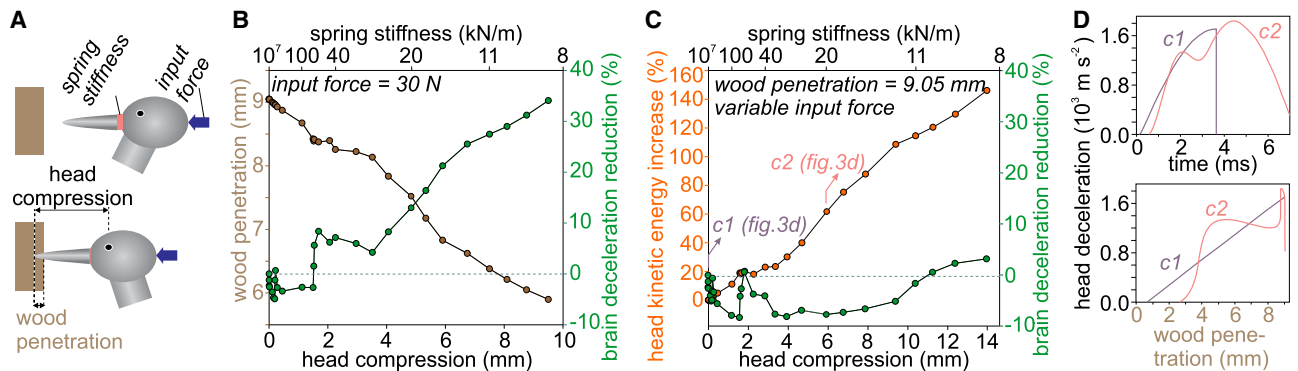
Figure 3. Effect of hypothetical shock absorption on pecking performance and braincase deceleration

For a Figure360 author presentation of figure 3, see the figure legend at https://doi.org/10.1016/j.cub.2022.05.052.

(A) The mathematical model's head and neck configuration at the start (top, two model input parameters indicated) and at maximum wood penetration (bottom, two output variables indicated).

(B) Simulations with equal head impulse (constant force input; equal speed at impact) for a range of spring stiffness at the beak-braincase interface (top scale), showing the trade-off between wood penetration depth (brown circles) and brain deceleration reduction relative to the value for maximally stiff crania (green circles) (see also Video S2, first half).

(C) Simulations achieving equal wood penetration depth by modifying head impulse (input force varies from 30 to 49 N; variable speed at impact), showing increasing kinetic energy requirement (orange circles; relative to maximally stiff crania) when more compression is allowed between beak and braincase (see also Video S2, final half).

(D) The observed increases in peak brain deceleration with increasing head compression are further explored for cases $c1$ (purple; maximal stiffness, velocity at impact 3.80 m s^{-1}) and $c2$ (pink; stiffness 20,000 N m^{-1}, velocity at impact 4.83 m s^{-1}). A late deceleration peak in $c2$, surpassing the peak of the simulation without cranial shock absorption, $c1$, is shown.

See also Video S2.

decreasing the brain's safety factor. Nevertheless, even subconcussion head impacts may call for brain trauma prevention or repair mechanisms within the braincase in the case of a repeated occurrence.[30] Such mechanisms include brain slosh reductions by the observed limited cerebrospinal fluid space of woodpeckers,[4] hypothesized neck vein compression to increase cranial blood pressure,[31,32] and damage repair by the observed proteins for stabilizing neuronal microtubules in the frontal lobes of woodpecker brains.[21]

While these insights expose a long-standing misconception about the presence of shock absorption in woodpeckers, which has infiltrated both common belief[33] and scientific research,[11,14–16] they open up a range of new questions about cranial function. How do woodpeckers manage to achieve this high stiffness in their cranial system, which includes a lower beak that can depress and retract, as well as an upper beak that has retained the capacity to rotate in the sagittal plane about the naso-frontal hinge (Figure 1)? A lock to limit dorsal flexion of
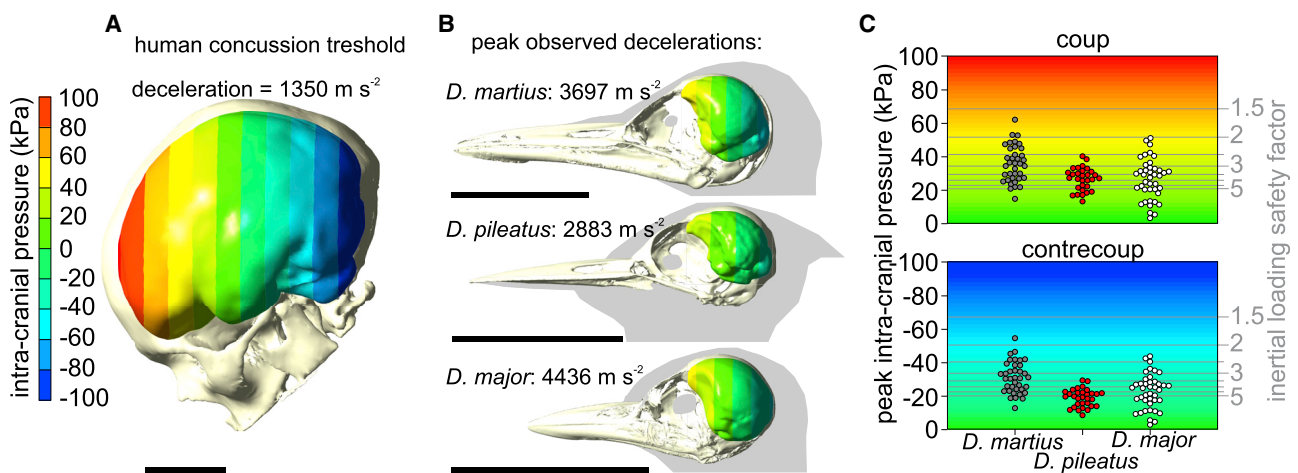

Figure 4. Comparison of intracranial pressure due to inertial loading between humans and woodpeckers

For a Figure360 author presentation of figure 4, see the figure legend at https://doi.org/10.1016/j.cub.2022.05.052.

Computed brain cavity surface pressures are shown for (A) an adult human at the concussion threshold deceleration and (B) the three woodpecker species at their measured peak deceleration of the eye. Peak coup (top graph) and contrecoup (bottom graph) pressures of separate hits (spheres) are shown in (C), including a scale (right axis) corresponding to the ratio of the concussion threshold pressure to the occurring pressure as an estimate of brain loading safety factor. Scale bars, 50 mm.

the upper beak has been identified,[5] but how is ventral flexion avoided? How is the suspension of the lower beak fixed during pecking? Consequently, our study opens new avenues for research to help us understand the mechanics behind cranial stiffening during pecking in birds.

STAR★METHODS

Detailed methods are provided in the online version of this paper and include the following:

- KEY RESOURCES TABLE
- RESOURCE AVAILABILITY
  - Lead contact
  - Materials availability
  - Data and code availability
- EXPERIMENTAL MODEL AND SUBJECT DETAILS
- METHOD DETAILS
  - Computed tomography
  - High-speed videography
  - Kinematic analysis
  - Mathematical models of pecking
  - Computational models of intracranial pressure
- QUANTIFICATION AND STATISTICAL ANALYSIS

AUTHOR CONTRIBUTIONS

S.V.W., E.J.O., R.E.S., and A.A. conceived the experimental design; all authors contributed to video data collection. S.V.W. and M.M. processed the raw data to extract detailed kinematics. S.V.W. performed the model simulations. C.B. and E.J.O. collected and processed the scan and morphometric data. S.V.W. drafted the manuscript; all authors contributed to data interpretation and manuscript preparation.

DECLARATION OF INTERESTS

The authors declare no competing interests.

REFERENCES

1. Bock, W.J. (1964). Kinetics of the avian skull. J. Morphol. *114*, 1–41. https://doi.org/10.1002/jmor.1051140102.

2. Beecher, W.J. (1953). Feeding adaptations and systematics in the avian order Piciformes. J. Wash. Acad. Sci. *43*, 293–299.

3. Spring, L.W. (1965). Climbing and pecking adaptations in some North American woodpeckers. Condor *67*, 457–488. https://doi.org/10.2307/1365612.

4. May, P.R.A., Fuster, J.M., Newman, P., and Hirschman, A. (1976). Woodpeckers and head injury. Lancet *1*, 454–455. https://doi.org/10.1016/s0140-6736(76)91477-x.

5. Bock, W.J. (1999). Functional and evolutionary morphology of woodpeckers. Ostrich *70*, 23–31. https://doi.org/10.1080/00306525.1999.9639746.

6. Schwab, I.R. (2002). Cure for a headache. Br. J. Ophthalmol. *86*, 843. https://doi.org/10.1136/bjo.86.8.843.

7. Oda, J., Sakamoto, J., and Sakano, K. (2006). Mechanical evaluation of the skeletal structure and tissue of the woodpecker and its shock absorbing system. JSME Int. J. Ser. A *49*, 390–396. https://doi.org/10.1299/jsmea.49.390.

8. Zhu, Z.D., Ma, G.J., Wu, C.W., and Chen, Z. (2012). Numerical study of the impact response of woodpecker's head. AIP Adv. *2*, 042173. https://doi.org/10.1063/1.4770305.

9. Wang, L., Cheung, J.T.-M., Pu, F., Li, D., Zhang, M., and Fan, Y. (2011). Why do woodpeckers resist head impact injury: a biomechanical investigation. PLoS ONE *6*, e26490. https://doi.org/10.1371/journal.pone.0026490.

10. Zhu, Z., Zhang, W., and Wu, C. (2014). Energy conversion in woodpecker on successive peckings and its role on anti-shock protection of the brain. Sci. China Technol. Sci. *57*, 1269–1275. https://doi.org/10.1007/s11431-014-5582-5.

11. Liu, Y., Qiu, X., Zhang, X., and Yu, T.X. (2015). Response of woodpecker's head during pecking process simulated by material point method. PLoS ONE *10*, e0122677. https://doi.org/10.1371/journal.pone.0122677.

12. Wang, L., Niu, X., Ni, Y., Xu, P., Liu, X., Lu, S., et al. (2013). Effect of microstructure of spongy bone in different parts of woodpecker's skull on resistance to impact injury. J. Nanomater. *2013*, 924564. https://doi.org/10.1155/2013/924564.

13. Yoon, S.-H., and Park, S. (2011). A mechanical analysis of woodpecker drumming and its application to shock-absorbing systems. Bioinspir. Biomim. *6*, 016003. https://doi.org/10.1088/1748-3182/6/1/016003.

14. Yoon, S.-H., Roh, J.-E., and Kim, K.L. (2009). Woodpecker-inspired shock isolation by microgranular bed. J. Phys. D: Appl. Phys. *42*, 035501. https://doi.org/10.1088/0022-3727/42/3/035501.

15. Bian, J., and Jing, X. (2014). Biomimetic design of woodpecker for shock and vibration protection. In 2014 IEEE International Conference on Robotics and Biomimetics (ROBIO 2014), pp. 2238–2243.

16. Horstemeyer, M.F. (2017) Shock mitigating materials and methods utilizing spiral shaped elements. US patent US9726249 B2, filed May 5, 2012, and granted August 8, 2017.

17. Kilham, L. (1959). Behavior and methods of communication of pileated woodpeckers. Condor *61*, 377–387. https://doi.org/10.2307/1365307.

18. Gibson, L.J. (2006). Woodpecker pecking: how woodpeckers avoid brain injury. J. Zool. *270*, 462–465. https://doi.org/10.1111/j.1469-7998.2006.00166.x.

19. Becher, F. (1953). Untensuchungen an Spechten zur Frage der funktionellen Anpassung und die mechanische Belastung. Z. Naturforschg *8b*, 192–203. https://doi.org/10.1515/znb-1953-0405.

20. May, P.R.A., Fuster, J.M., Haber, J., and Hirschman, A. (1979). Woodpecker drilling behavior. An endorsement of the rotational theory of impact brain injury. Arch. Neurol. *36*, 370–373. https://doi.org/10.1001/archneur.1979.00500420080011.

21. Farah, G., Siwek, D., and Cummings, P. (2018). Tau accumulations in the brains of woodpeckers. PLoS ONE *13*, e0191526. https://doi.org/10.1371/journal.pone.0191526.

22. King, A.I. (2018). The Biomechanics of Impact Injury (Springer International Publishing AG).

23. Jung, J.-Y., Pissarenko, A., Trikanad, A.A., Restrepo, D., Su, F.Y., Marquez, A., et al. (2019). A natural stress deflector on the head? Mechanical and functional evaluation of the woodpecker skull bones. Adv. Theory Simul. *2*, 18001852. https://doi.org/10.1002/adts.201800152.

24. Salem, S.A.L., Al-Hassani, S.T.S., and Johnson, W. (1975). Aspects of the mechanics of driving nails into wood. Int. J. Mech. Sci. *17*, 211–225. https://doi.org/10.1016/0020-7403(75)90054-5.

25. Liu, Y., Qiu, X., Ma, H., Fu, W., and Yu, T.X. (2017). A study of woodpecker's pecking process and the impact response of its brain. Int. J. Impact Eng. *108*, 263–271. https://doi.org/10.1016/j.ijimpeng.2017.05.016.

26. Thomas, L.M., Roberts, V.L., and Gurdjian, E.S. (1966). Experimental intracranial pressure gradients in the human skull. J. Neurol. Neurosurg. Psychiatr. *29*, 404–411. https://doi.org/10.1136/jnnp.29.5.404.

27. Ono, K., Kikuchi, A., Nakamura, M., Kobayashi, H., and Nakamura, N. (1980). Human head tolerance to sagittal impact reliable estimation deduced from experimental head injury using subhuman primates and human cadaver skulls. SAE Technical Paper 801303.

28. Ni, Y., Wang, L., and Fan, Y. (2017). Mechanical properties of triple periodic minimal surface structures mimicking the microstructure of woodpecker's cranial bone. Conf. Proc. IEEE Eng. Med. Biol. Soc. *2017*, 1873–1876. https://doi.org/10.1109/EMBC.2017.8037212.

29. Puverel, C., Abourachid, A., Böhmer, C., Leban, J.-M., Svoboda, M., and Paillet, Y. (2019). This is my spot: what are the characteristics of the trees excavated by the black woodpecker? A case study in two managed French forests. Forest Ecol. Manag. *453*, 117621. https://doi.org/10.1016/j.foreco.2019.117621.

30. Bailes, J.E., Petraglia, A.L., Omalu, B.I., Nauman, E., and Talavage, T. (2013). Role of subconcussion in repetitive mild traumatic brain injury. J. Neurosurg. *119*, 1235–1245. https://doi.org/10.3171/2013.7.JNS121822.

31. Smith, D.W., Bailes, J.E., Fisher, J.A., Robles, J., Turner, R.C., and Mills, J.D. (2011). Internal jugular vein compression mitigates traumatic axonal injury in a rat model by reducing the intracranial slosh effect. Neurosurgery *70*, 740–746. https://doi.org/10.1227/NEU.0b013e318235b991.

32. Myer, G.D., Yuan, W., Barber Foss, K.D., Smith, D., Altaye, M., Reches, A., et al. (2016). The effects of external jugular compression applied during head impact exposure on longitudinal changes in brain neuroanatomical and neurophysiological biomarkers: a preliminary investigation. Front. Neurol. *7*, 74. https://doi.org/10.3389/fneur.2016.00074.

33. O'Connor, M. (2007). Why Don't Woodpeckers Get Headaches? (Beacon Press).

34. Goswami, A. (2015). Phenome10K: a free online repository for 3-D scans of biological and palaeontological specimens. https://www.phenome10k.org.

35. Erer, K.S. (2007). Adaptive usage of the Butterworth digital filter. J. Biomech. *40*, 2934–2943. https://doi.org/10.1016/j.jbiomech.2007.02.019.

36. Nahum, A.M., Smith, R., and Ward, C.C. (1977). Intracranial pressure dynamics during head impact. SAE Technical Paper 770922.

STAR★METHODS

KEY RESOURCES TABLE

REAGENT or RESOURCE	SOURCE	IDENTIFIER
Deposited data		
All videos, raw kinematic data, and source and output from the mathematical models	This paper; Mendeley data	https://doi.org/10.17632/w5vnd3z4xd.1
Software and algorithms		
Didge 2.3	A. Cullum, Creighton University, Omaha	http://biology.creighton.edu/faculty/cullum/Didge
XMAlab 1.5.5	B. Knörlein, Brown University, Rhode Island	https://bitbucket.org/xromm/xmalab/downloads/
VBA Excel Butterworth Filter	S. Van Wassenbergh, University of Antwerp	www.uantwerpen.be/en/staff/sam-vanwassenbergh/my-website/excel-vba-tools/
Simscape Multibody v. 5.0	Mathworks, Natick, USA	https://mathworks.com/products/simscape-multibody.html
MeshLab	Visual Computing Lab ISTI-CNR	https://www.meshlab.net/
Avizo v.6.3	Visualization Science Group, Mérignac, France	https://www.thermofisher.com/avizo.html
ANSYS 2020 R1	Ansys, Canonsburg, USA	https://www.ansys.com/
Past 4.04	Øyvind Hammer, University of Oslo, Norway	https://www.nhm.uio.no/english/research/infrastructure/past/
Sigmaplot 11.0	Systat Software, San Jose, USA	http://www.sigmaplot.co.uk/
Geomagic Wrap 2017	3D Systems, Rock Hill, USA	https://www.3dsystems.com/software/geomagic-wrap

RESOURCE AVAILABILITY

Lead contact
Further information and requests for resources and reagents should be directed to and will be fulfilled by the Lead Contact, Sam Van Wassenbergh (sam.vanwassenbergh@uantwerpen.be)

Materials availability
This study did not generate new unique reagents.

Data and code availability
All original data and code has been deposited at Mendeley Data and is publicly available as of the date of publication. DOIs are listed in the key resources table.

EXPERIMENTAL MODEL AND SUBJECT DETAILS

One adult *Dryocopus martius* (individual 1) was filmed in Alpenzoo Innsbruck (Austria). A second (individual 2) was filmed in Tierpark Goldau (Switserland). *Dendrocopos major* individuals were filmed in Tierpark Riesa, Germany (individual 1), and in Oasi di Sant' Alessio, Italy (individual 2). Two individuals of *Dryocopus pileatus* were filmed in a laboratory setting at British Columbia University after being captured using mist nets in British Columbia on private property with landowner permission, using suet feeders, decoys, and calls replays. While housed at the Centre for Comparative Medicine, they were kept in large cages enriched with boxes, perches, and rotting logs. The woodpeckers were fed a daily diet of suet, egg yolks, berries, live meal worms, a mixture of chick starter feed and wet dog food, and mixed nuts. This work on *D. pileatus* was carried out under University of British Columbia Animal Care Certificate #4981-12, Scientific Permit to Capture and Band Migratory Birds 10844A, and Canadian Wildlife Services Permit to Capture/Kill for Scientific Purposes BC-13-0047. Head size, defined as the distance between the tip of the beak and the back of the head following the centreline of the beak, was measured either from pictures of the head at the level of a reference grid (*D. martius* and *D. major*), or from a calibration object placed in the field of view (*D. pileatus*). Head lengths, for individuals 1 and 2, respectively, were 116.4 mm and 123.0 mm for *D. martius*, 90.2 mm and 105.1 mm for *D. pileatus*, and 68.2 mm and 75.2 mm for *D. major*.

METHOD DETAILS

Computed tomography

The heads of a black woodpecker (*Dryocopus martius*) and a great-spotted woodpecker (*Dendrocopos major*) with neck attached were scanned in situ with surrounding soft-tissue using micro-computer tomography (μCT) (RX Solutions EasyTom Micro, Annecy, France; 315μA; 80kV; voxel size of 43 μm). The cranium of a pileated woodpecker (*Dryocopus pileatus*) was scanned immediately after euthanasia using a Bruker Biospec7 Tesla magnetic resonance imaging scanner (Bruker BioSpin Corporation, Billerica, MA, USA). The 3D models were reconstructed from the μCT using Avizo (Version 6.3, Visualization Science Group, Mérignac, France) and MeshLab (ISTI-CNR, Pisa, Italy). A skeletal reconstructions of *D. pileatus* from the Phenome10k repository[34] is used for visualization purposes (Figure 4B).

High-speed videography

High-speed videos of *Dryocopus martius* in lateral view during pecking were recorded in an uncompressed 10-bit monochrome format using a Mikrotron Eosens TS3 camera (Mikrotron GmbH, Unterschleissheim, Germany). *D. martius* individual 1 was filmed at 2698 frames/s for 512 × 410 pixels, and individual 2 at 4000 frames/s for 402 × 322 pixels. Both individuals were pecking hard-wood tree trunks of about 0.3 m in diameter. *Dendrocopos major* individual 2 was filmed at 3000 frames/s using the Mikrotron camera for 480 × 384 pixels while pecking on a bamboo stick that was firmly attached to the cage, and individual 1 pecking filmed pecking on 0.2 m diameter hardwood trunks using a Fastec IL5 camera (Fastec Imaging, San Diego, CA, USA) for 654 x 436 pixels. Shutter speeds were set to the inverse of the frame rate. Prior to the filming sessions of *Dryocopus pileatus*, the birds were transferred to smaller mesh-topped acrylic boxes using butterfly nets. Color videos (uncompressed 32-bits) were made from lateral view using a Phantom Miro M120 camera at 1600 frames/s at 1280 × 800 or 1024 × 768 pixels during pecking on spruce beams.

Kinematic analysis

In total, 109 pecks were analyzed: 21 and 16 for the two *D. martius* individuals, 22 and 9 for the two *D. pileatus* individuals, and 22 and 19 for the two *D. major* individuals. Head size, defined as the distance between the tip of the beak and the back of the head following the centerline of the beak, was measured either from pictures of the head at the level of a reference grid (*D. martius* and *D. major*), or from a calibration object placed in the field of view (*D. pileatus*). Head lengths, for individuals 1 and 2, respectively, were 116.4 mm and 123.0 mm for *D. martius*, 90.2 mm and 105.1 mm for *D. pileatus*, and 68.2 mm and 75.2 mm for *D. major*.

For all analyzed videos, the coordinates of several anatomical landmarks were determined on each frame in a minimally 12 ms period with the instant of beak impact approximately in the middle of the frame sequence using Didge 2.3 (Alistair Cullum, Creighton University, Omaha) or XMAlab 1.5.5 (B. Knörlein, Brown University, Rhode Island). Three landmarks (Figure 2A; Video S1) were tracked in all videos: (1) a spot on the upper beak that lies approximately central along the length of the beak, and is, therefore, referred to as the "middle beak" landmark. In *D. martius*, this was the tip of the sharp, anterior-pointing triangle-shaped zone covered with black feathers on the dorsal side of the upper beak. In the other species, smaller contrasting spots could be identified and selected for tracking at this location; (2) a point at the posterior end of the upper beak, which is referred to as the "posterior beak" landmark. In *D. martius*, this was the tip of the posterior-pointing, sharp triangle of light keratin at about half of beak height. In the other species, distinct edges of the feather coverage were selected in the posterior beak region; and (3) the center of the eye or a fixed point at the edge of the eye. In the majority of video of *D. pileatus* (15 out of 22 in individual 1; 9 out of 9 in individual 2) a fourth landmark was tracked as well: (4) a white dot on the right side of their heads behind the eye after feathers were clipped down to the skin, which was referred to as the "skull" landmark. All landmarks were tracked three times using different image brightness and contrast settings yielding a suitable view for tracking, and the mean was used in further analyses.

Next, as movement approximately occurs along a linear path, a new axis was defined (x') parallel to the direction of motion. This direction of motion was determined from the first to the fifth frame of each analyzed image sequence (Figure S1). All reported velocities and accelerations are along this new x'-axis. After setting the time of peak deceleration to zero, averaging velocities and accelerations between hits yielded largely similar kinematic profiles for the two individuals per species, which confirms the absence of aberrant behaviour by our specimens studied (Figure S2).

As random error in landmark position determination is inevitable, this "noise" must be reduced before velocities and accelerations can be calculated. In order to avoid underestimation of acceleration peaks, we used a low-pass filter specifically developed for the analysis of impact events: Erer's adaptive Butterworth filter.[35] This digital filter has a variable cut-off frequency distribution defined for each data point, which is determined by local signal characteristics. The algorithm was allowed to determine the most appropriate, instantaneous cut-off frequency from a range that was set in function of recording frame rate and noise level based on visual inspection of the filtered profiles. Ranges 250-750 Hz, 300-600 Hz, and 400 to 1000 Hz were used for, respectively, *D. martius*, *D. pileatus*, and *D. major*. Visual inspection of the results showed that this noise-reduction filter outperformed more commonly used fourth-order recursive low-pass Butterworth filters with a constant cut-off frequency (see Figure S1). Note that since the duration of the impact phase was approximately 4 ms, the relatively high temporal resolution of our high-speed videos allowed us to sample the deceleration phase with at least 6 points for *D. pileatus*, and more than 12 for *D. martius* and *D. major*; therefore, discretization error should be small. As a measure of landmark tracking precision, we calculated the standard deviation of the distance between the middle beak and eye landmarks for the first 10 frames for each video when the head was in the approach phase. This estimate is conservative as it assumes complete rigidity between these two landmarks at this time, and may include stronger effects of motion blur than during the

impact phase due to the higher velocity of the head before impact. The mean (± standard deviation) estimated precisions were 0.26 ± 0.14 mm (*D. martius* individual 1), 0.15 ± 0.11 mm (*D. martius* individual 2), 0.41 ± 0.27 mm (*D. pileatus* individual 1), 0.19 ± 0.10 mm (*D. pileatus* individual 2), 0.07 ± 0.05 mm (*D. major* individual 1), and 0.10 ± 0.05 mm (*D. major* individual 2). According to the presented mathematical models (Figure 3), these values are well below the amount of compression to achieve even a small reduction of 5% in the brain's peak deceleration (either about 3 mm or >14 mm depending on the performance target; see Figures 3B and 3C). Random variation in kinematic variables caused by precision limitation are accounted for by statistics applied to the multiple impacts analyzed per individual (see below).

Mathematical models of pecking

The penetration of the black woodpecker's beak into the wood was mathematically simulated with a forward dynamic, multi-body model using Simscape Multibody v 5.0 (Mathworks, Natick, USA). The moving body parts at the time of impact, namely the head and upper part of the neck, were modeled as three rigid bodies of simplified shapes (Figure S4A): (1) a prolate spheroid mimicking the beak, (2) an ellipsoid representing the braincase, and (3) a cylinder representing the upper region of the neck. The dimensions of these 3-D shapes were measured on the dorsal and lateral images of *D. martius* individual 1 used in the kinematic analysis.

To estimate an overall density of these modeled head volumes, a skull of an in alcohol preserved *D. martius* specimen was wet-weighed (15.5 g) and scaled isometrically to match the size of individual 1 (length scale factor 1.27). Twelve percent extra mass was added to account for the skin, feathers, and eyes. Dividing the resulting 35.5 g by the summed braincase and beak volume yielded the used density of 750 kg m^{-3}. Three joints allowed movement of the modeled head (Figure S4B): The beak and braincase can translate relative to each other along the length axis (*joint 1*). The resistance to do so was modeled as a linear spring with stiffness K_{head}. The head is free to rotate about the neck in the sagittal plane (*joint 2*). The neck is also allowed to rotate, but a prismatic joint keeps the center of the base plane at a vertical axis (*joint 3*). K_{head} was varied to evaluate the effects of the degree of head compression upon impact.

The model was set in motion by a constant input force on the braincase, mimicking the force transmitted from the neck to thrust the head forward (Figure S4B). Except for the simulations where the kinetic energy was increased (Figure 3C), this force was set to 30 N as this resulted in a realistic peak acceleration of 477 m s^{-2} (Figure S2). The modeled impact with the wood was set to start at the time the head reached 3.8 m s^{-1}, the overall mean impact velocity measured in our study for *D. martius*. As soon as the beak tip enters the wood, it experiences a wood-reaction force that increases linearly with the depth of penetration (Figure S4). This formulation corresponds to a simple mathematical model of a straight-tapered tip of a nail penetrating wood.[24] The stiffness constant K_{wood} describes the slope of this linear increase in wood-counterforce with penetration depth. This constant was fine-tuned to achieve a realistic peak deceleration of 1.7 10^3 m s^{-2}, and a realistic deceleration duration of 3.7 ms (Figure S2) by setting it to 13000 N m^{-1}.

To simplify the model interpretation, a first set of simulations were performed without including any dampening (i.e., velocity-dependent resistance that dissipates as heat loss) in *joint 1*. This means that all mechanical energy either remained in the multi-body system (kinetic energy and elastically stored energy in the beak-braincase joint) or went into plastic deformation of the wood. A significant elastic component in the hypothetical shock absorber seems required to ensure a quick restoring for successive pecking (commonly 2 to 3 pecks per second were observed). Additionally, to test whether dashpot-like damping, for example, as part of visco-elastic behaviour, would affect the deceleration of the braincase during the beak's penetration of the wood, a second set of simulations were run (Figure S5). In that case, the stiffness at *joint 1* was set to zero, and the damping coefficient varied from extremely high (5000 N (m/s)$^{-1}$) to lower values resulting in substantial compression during beak impact. As both hypothetical extremes, a purely elastic spring system (Figure 3) and a purely viscous damping system (Figure S5), could not reduce brain deceleration for pecks of equal penetration depth, this result will also apply to any combinations of these two performing visco-elastic damping.

The model was solved using the Runge-Kutta (ode4) solver with a fixed time-step size of 0.001 ms. The robustness of the solution was confirmed by observing negligible differences when using smaller time steps (0.0001 ms) on a different differential equation solver (ode3 Bogacki-Shampine).

Computational models of intracranial pressure

The effect of size, shape and deceleration magnitude on inertia-driven intracranial pressure changes was evaluated by comparing the hydrodynamic pressure of a water-filled, enclosed human braincase at the deceleration threshold for concussions (which is about 1350 m s^{-2} for an impact duration of 4 ms)[22] to that of the three woodpecker species woodpecker at their observed maximal deceleration. In analogy with standard head impact tests,[36] the human reference for frontal impact simulation was performed with the head's Frankfort anatomical plane inclined 45° to the horizontal. The braincase surface was extracted from a CT scan-based, anonymized adult human skull surface mesh ID 3DPX-002727 from the NIH 3D printing database (U.S. Department of Health and Human Services, Bethesda, USA). After converting to spline surfaces using Geomagic Wrap (version 2017, 3D Systems, Rock Hill, USA), the braincase volume was meshed with about 200 000 tetrahedra using ANSYS Meshing (version 2020 R1, Ansys, Canonsburg, USA).

A transient model of backward acceleration was solved using the density-based computational fluid dynamics solver of ANSYS Fluent 2020 R1. We used the solver settings recommended by default (i.e., implicit formulation; Roe-FDS Flux type, least-squares cell-based gradient discretisation, second order upwind scheme for flow discretization). A constant acceleration was imposed by a user-defined function. The model was solved for 3 time steps using 500 iterations per time step, which safely reached iterative convergence. As this translation of a closed vessel filled with a fluid of a uniform density, no fluid motion occurred relative to the

moving boundaries of the brain cavity, and hence the calculations were insensitive to changes in both mesh and solver settings. This procedure was repeated for the brain cavities of the woodpeckers from our CT or MRI scans (Figure 4). Brain cavity reconstruction were scaled isometrically to match the size of the individuals from the kinematic analysis, and simulations were run for the corresponding individual's observed maximum of eye deceleration. Intracranial pressure data for additional hits presented in Figure 4C were derived by linear interpolation based on the difference in deceleration magnitude. The summed hydrodynamic forces of the brain surface mesh triangles properly obeyed Newton's law for acceleration-reaction force with a maximal deviation of 0.15%, which illustrates the high resolution of all simulations.

QUANTIFICATION AND STATISTICAL ANALYSIS

Paired t tests were performed on deceleration magnitudes of different landmarks on the head using Sigmaplot 11.0 (Systat Software, San Jose, USA). The assumption of normality was tested for pairwise differences in deceleration, which passed the Shapiro-Wilk normality test, except for a single case for which a Wilcoxon Signed Rank Test was performed (Table S1). No clear outliers were detected in box plots (see also Figure 2A). Reduced major axis regressions were used to determine the relationship between deceleration magnitudes of different landmarks, as this type of regression is suited to cases where both variables are subject to measurement error. Ninety-five percent confidence intervals are determined by bootstrapping with 1999 replicates. This regression analysis was performed using Past 4.04 (Øyvind Hammer, University of Oslo, Norway).